Terahertz beam steering using active diffraction grating fabricated by 3D printing

JOHANNES M. SEIFERT,[1] GORETTI G. HENANDEZ-CARDOSO,[2] MARTIN KOCH[2] AND ENRIQUE CASTRO-CAMUS[2,*]

[1] *Faculty of Physics and Material Sciences Center, Philipps-Universitat Marburg, Renthof 5, 35032, Marburg, Germany.*
[2] *Centro de Investigaciones en Optica A.C., Loma del Bosque 115, Lomas del Campestre, Leon, Guanajuato, 37150, Mexico.*
[*] *enrique@cio.m*

Abstract: In this article we propose variable-period diffraction gratings for terahertz frequencies. The design, fabrication and characterization of such devices are presented. Our measurements show the possibility to actively shift of the deflection angle for each frequency using this device. We also demonstrated that when driven by a speaker, these variable gratings can be used for active beam steering with potential application in terahertz communications.

1. Introduction

Terahertz (THz) technology has evolved dramatically since the introduction of Time-Domain Spectroscopy (TDS) in the 1980s [1,2]. This technique made it possible to access the entire band between about 30 GHz and 10 THz in a single experimental technique. Since then, electronic sources of radiation such as Gunn diodes, and other forms of oscillators have gradually increased the available frequencies covering most of the low end of this band [3,4]. Simultaneously optical sources such as quantum cascade lasers have also been produced at progressively lower frequencies [5,6]. While there are still technological challenges for the two kinds of technologies to be commercially available for mass markets, these development have paved the road for the use of terahertz radiation in many real-world applications that go from cultural heritage [7–9], biomedical [10–14] and industrial non-destructive testing [15,16] to short range ultra-broad-band telecommunications [17–20].

Fundamental estimations for short-range wireless THz communication systems show that such systems will need a line-of-sight connection between receiver and emitter. To circumvent the blocking of the direct line-of-sight connection these systems will also have to rely on non-line-of-sight paths which involve reflections off the walls. This requires beam steering, which will enable securing reliable communication paths even when the emitters or receivers are changing their positions or objects interrupt the line-of-sight link. Although several approaches have been demonstrated, including a freely programmable THz diffraction grating [21], vanadium dioxide metasurfaces [22], a liquid crystal prism [23], optically excited semiconductors [24,25], interference of femtosecond optical pulses [26], and optical coherent control [27], THz beam steering is still in its infancy.

Given that THz is still a relatively unexplored part of the spectrum, the availability of electronic, optical and hybrid components for this band is still limited [28]. In recent years, three-dimensional printing has been used to fabricate many standard [29,30] and also unconventional [31–33] optical components for THz waves, including gratings [34–40]. Three-dimensional printing has considerable advantages for prototyping, the time from design to final fabrication can be as short as a few minutes, the training required to use it is fast and easy to acquire, the operation costs are very low and the flexibility of the technique is extremely high. Furthermore, there are many 3D printable plastics that show good optical properties at THz frequencies [28,41].

In addition to the advantages of 3D printing as a prototyping technique, the designs fabricated with this technique for initial testing and optimization can, in most cases, easily be converted to mold-injection fabrication for their mass production.

An interesting aspect of plastic-based optical components is the fact that they can be designed to be elastic, which opens the possibility to create active components. In this contribution we present an elastic diffraction grating, our design is such that the period of the grating can be modified in order to either select a particular frequency for a given diffraction angle or modify the diffraction angle for a given frequency. The first characteristic can be useful for spectroscopic purposes or as a tunable filter, while the later one could be useful for beam steering in telecommunications or other applications.

2. Design and fabrication

A reflective diffraction grating produces diffracted beams at a series of angles with respect to the normal to the grating given by

$$\frac{\Lambda}{\lambda}\sin\theta_m = m, \tag{1}$$

where Λ is the period of the grating, λ is the wavelenght, θ_m is the diffraction angle with respect to the grating's normal and $m = \pm 1, \pm 2, \ldots$ is the diffraction order. From the previous equation it is easy to show that for the first diffraction order

$$\sin\theta_1 = \frac{c}{\Lambda}\frac{1}{f}, \tag{2}$$

where f is the frequency of the electromagnetic wave and c is the speed of light. This implies that the relationship between the frequency of the wave and its corresponding diffraction angle can be tuned if the period Λ can be actively controlled.

We fabricated a reflective diffraction grating, formed by a sequence of 17 stripes of material of lenght 50 mm, width 0.8 mm and height 0.8 mm joined by V-shaped "springs" at the edges as shown in Fig. 1. When completely relaxed, the spacing between subsequent stripes is ~2.3 mm which can be continuously reduced down to ~1.1 mm by applying lateral pressure normal to the stripes. Since all springs are, at least nominally, equal, the compression is expected to affect evenly the spacing between all the stripes. Before printing we placed aluminium foil on the bed of the 3D-printer, therefore depositing the plastic structure on the foil. After printing, the metal that was attached directly to the plastic was maintained while the rest was removed. With this we managed to obtain a highly reflective layer on top of the plastic structure. The RMS roughness of the metal edges was determined to be ~19.4 μm.

In addition to the grating itself, the three-dimensional printer was also used to fabricate a vice mount appropriate to control the compression on the grating which is shown in Fig. 1 The compression can be modified precisely by using a screw that varies the total length of the grating. By inspecting photographs of the grating at different compression levels we could asses that the compression is reasonably well distributed over the 17 periods of the grating going from a variation (standard deviation) of about 3 % (~ 70 μm) on the period for the uncompressed grating up to about 8 % (~ 140 μm) for the most compressed case.

A second grating with a similar geometry formed by a sequence of 19 stripes of material of length 80 mm, width 1.5 mm and height 10 mm optimal for frequencies in the vicinity of 120 GHz was also fabricated together with an appropriate mount for this re-scaled version, the thickness increased significantly in order to make the structure more stable for fast compression.

3. Characterization

We used a fiber-coupled terahertz time-domain spectrometer in order to characterize the tunable gratings. A polyethylene lens was used to collimate the radiaiton produced at the emitter.

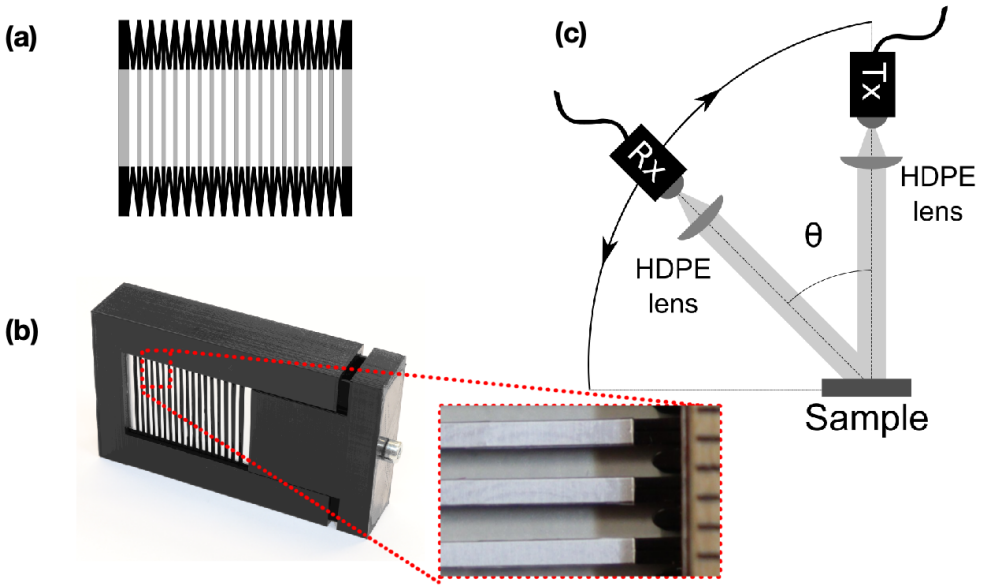

Fig. 1. (a) Photograph of the free-standing grating as printed. (b) Photograph of the grating in its pressing mount, a closeup image of three periods of the grating with a reference scale on the right-hand-zise (1 mm per line) is provided. (c) Schematic of geometry of the THz optical path the receiver and its corresponding lens is mounted on a motorized goniometer in order to vary the detection angle.

Subsequently the device under test was placed at the intersection of the optical axis of the emitter and the rotation axis of a motorized rotational stage fitted with a ~400 mm long arm where an additional lens and the photoconductive detector were placed as show in Fig. 1c. For all of our experiments the polarization was transverse to the grating slabs.

The device under test was smaller grating described earlier. It was mounted inside the variable compression system. In order to measure the behaviour of the grating a collection of terahertz waveforms were acquired for different angular positions of the detector between 30° and 55° of the detector arm in 0.5° steps. Subsequently, the compression of the grating was increased, thus reducing the period of the grating, and the measurements were repeated for a total of three different compressions (Λ =2.92 mm, 2.52 mm and 2.11 mm). The spectra resulting from all the measurements, obtained by Fourier transformation of the waveforms, are shown in Fig. 2a-c.

The spectra shown in Fig. 2a corresponds to the terahertz signals recorded for a collection of angular positions of the detector as described in the previous paragraph. The color intensity of each curve was chosen such that it increases with the detector angle. As seen in the plots, the peak frequency of the diffracted signal decreases as the detection angle increases. One can notice that the second diffraction order appears at higher frequencies (>225 GHz) and up to 5 diffraction orders spanning up to about 1 THz (not shown) could be found with decreasing amplitudes. In Figs. 2b and c, the results of analogous measurements are shown for increasing compression levels of the grating, ie. decreasing period lengths. The curves show that the spectral peaks appear at progressively larger frequencies as the grating gets compressed, which is consistent with Eq. 2. Finally, Fig. 2d shows a collection of points that correspond to the peak frequencies of all the spectra as function of the detection angle for the different compression levels, the solid curves shown are the predictions using Eq. 2. As observed in the plot there is good quantitative match between the theory and the experiment.

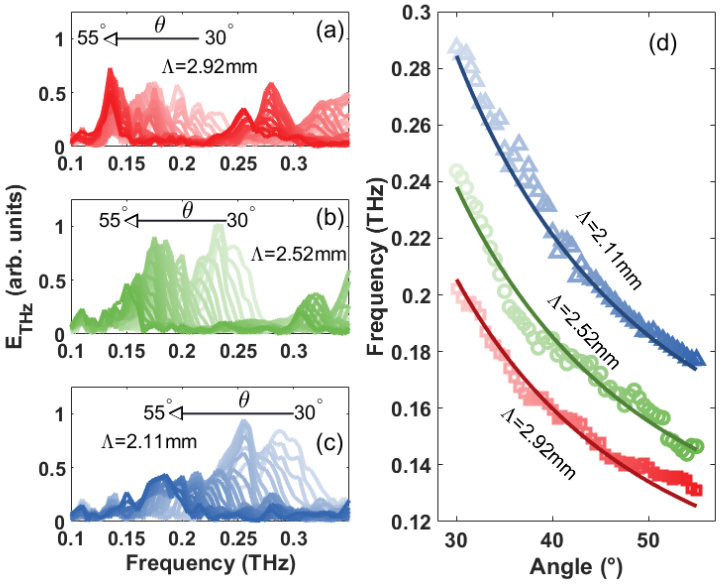

Fig. 2. (a) The spectra obtained for angles between 30° (lighter color) and 55° (darker color) in 0.5° steps for the grating at a compression state such that its period is 2.92 mm. The spectral peak clearly shifts as a function of the detection angle as indicated by the arrow, on the right hand side, additional peaks can be seen, which correspond the second diffraction order. (b) and (c) show analogous sets of spectra for compressions such that the period is 2.52 mm and 2.11 mm respectively, it is possible to notice that the collection of spectral peaks for the first diffraction order appear to higher frequencies as the period decreases. (d) The peak frequency of all the spectra shown in panels (a)=□, (b)=◯ and (c)=△ are ploted here. The continuous lines represent the relation between the frequency and the angle of the first diffraction order from Eq. 2.

A quick inspection of Fig. 2d allows noticing that a change of ~800 μm in the period of the grating, produces a deflection from ~35° to ~50° at 180 GHz. The period change could be driven by an electromagnetic or piezoelectric actuator, this could lead to a potential beam-steering device which we present in the next section.

4. Active beam steering

In order to test the possibility of active beam stearing a separate setup was prepared. The larger grating, optimized for 120 GHz operation, was placed in its mount, and the ensemble was fixed and coupled to an audio speaker in such a way that the oscillations from the speaker drive a compression/decompression motion on the grating. The speaker was driven by a sine wave applied from a function generator, as shown in Fig. 3a. Instead of a THz-TDS system we used a 120 GHz CW emitter and detector in a setup such as the one shown in Fig 3c. The length L of the detection arm, between the grating and the detector, was L=2.6 m. The signal from the detector was coupled to an oscilloscope triggered by the sine-wave driving the speaker as shown in Fig. 3b.

From the experimental points shown in Fig. 3a and b, which corresponds to a frequency of 60.5 Hz on the speaker, one can clearly see that the signal seen in the detector shows two maxima per speaker cycle, which is to be expected since the beam is steered forwards and then backwards, illuminating the detector twice in a single cycle. The theoretical curve shown in Fig.3b was calculated by assuming that the beam has a Gaussian profile, and that the response of

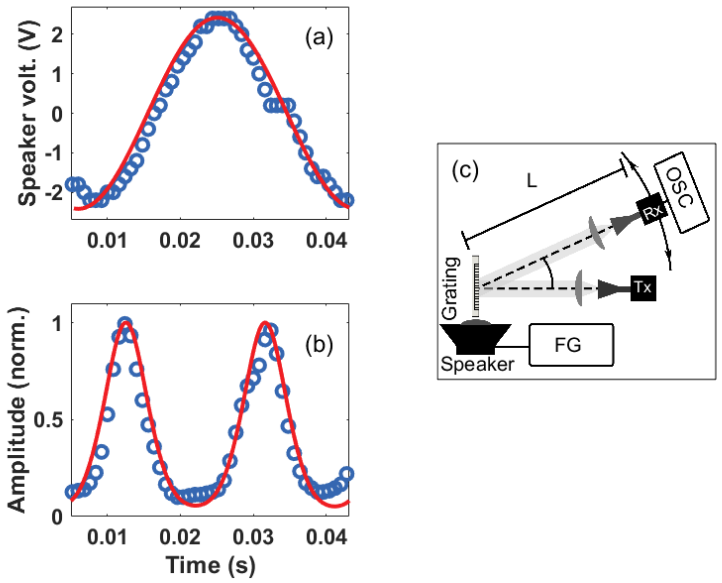

Fig. 3. (a) Voltage applied to the speaker at 60 Hz, (◯) one full cycle is shown. The continuous line is the displacement used for the calculation of the diffracted angle, the amplitude, phase and frequency were matched to the voltage signal for visualization purposes. (b) Amplitude of the signal obtained from the microwave detector with speaker being driven at 60.5 Hz (◯), and theoretical prediction of the amplitude detected shown as a continuous curve with a total angular deflection of 2.8° over the cycle. (c) Schematic of the setup including the speaker and microwave emitter and detector.

the lens-detector system is also Gaussian. For this calculation there are two important parameters that need being determined. Firstly, the beam cross section, and secondly the pitch variation of the grating owing to the oscillation. The beam cross-section in the vicinity of the detector-arm's lens was measured by the razor-blade scanning method and turned out to be σ=13.0 mm (30.6 mm FWHM). The variation of the grating pitch was obtained using long-exposure photographs of the grating while being driven by the speaker, by analyzing the blurred parts of the image it was possible to determine the total displacement of each stripe of the grating, and from there the change in pitch over the cycle which turned out to be from 3.09 mm to 3.20 mm, which in turn resulted in diffraction angles between $51.3° = 52.6° - 1.3° < \theta < 52.6° + 1.3° = 53.9°$. Taking these two parameters, the angle as well as the distance between the grating and the detector, the expected signal can be calculated as

$$s(t) = S_0 \int_{-\infty}^{+\infty} \int_{-\infty}^{+\infty} e^{\left(-\frac{(x-X(t))^2}{\sigma^2} + -\frac{(y-y_0)^2}{\sigma^2}\right)} e^{\left(-\frac{(x-x_0)^2}{\sigma_D^2} + -\frac{(y-y_0)^2}{\sigma_D^2}\right)} \mathrm{d}x\mathrm{d}y, \tag{3}$$

where $X(t) \sim x_0 + L\delta(t)$ and $\delta(t) = \delta_0 \cos(\omega_{\mathrm{spk}} t)$, with $\delta_0 = 1.3°$, $\omega_{\mathrm{spk}} = 2\pi \times 60.5$ Hz the speaker angular frequency and σ_D=34 mm defines the effective detector area. By using this expression we could predict the amplitude of the signal which appears in Fig. 3b as a continuous line that matches very well the experimentally measured signal. It is important to notice that the frequency of 60.5 Hz was chosen because the grating shows a mechanical resonance at that frequency. An other mechanical resonance was found at ~29 Hz with very similar results, and one more at ~112.5 Hz, however, that resonance only showed a smaller angular modulation,

which we attribute to a smaller displacement of the grating slabs. It is worth mentioning that the angular modulation is very small for frequencies that do not match a mechanical resonance.

5. Conclusions

In this article we proposed designs of variable-period diffraction gratings for terahertz frequencies. The devices were designed in such a way that compression in the direction orthogonal to the gratings' stripes produces an elastic, reversible and even change of the period along the entire structure. The design was subsequently fabricated by three-dimensional printing, and tested using a THz time-domain spectroscopy system. The measurements show, that application of constant pressure, produces a controllable shift of the deflection angle for each electromagnetic frequency, and the behaviour matches quantitatively with the theoretical equations used during the design. It is worth mentioning that the current resolution of Fused Material Deposition 3D printing is restricted to about 200 μm, which limits these kinds of devices to the frequency region of a few hundreds of gigahertz, however, the same concept could be applied to similar devices either using other three-dimensional printing technologies or different fabrication methods.

One of these gratings was tested by actively modulating the pressure with a speaker, resulting in an active beam steering device. It is worth mentioning that the active beam steering is most efficient at the frequencies where the grating shows mechanical resonances, therefore, if higher steering speeds are desired, mechanical changes, such as reduction of the mass of the grating, or an increase of the stiffness of the springs can be used to re-engineer the device. Furthermore, while we aimed to present a proof-of-concept, an actual device of this type could be driven with a more appropriate electromagnetic or piezoelectric actuator that could increase the modulation angles and speeds, which could make these simple plastic-based devices suitable for real-world applications such as THz telecommunications.

Funding

The authors would like to acknowledge the financial support of the Deutsche Forschungsgemeinschaft (grant KO 1520/17-1) and the Alexander von Humboldt Foundation through an Experienced Research Fellowship.

Contributions

The investigation was planned and supervised by ECC with support from MK. The initial design and fabrication of the devices was performed by JS. The optimization of the design was jointly done by JS and GGHC. The measurements were done by GGHC and JS. JS, GGHC and ECC prepared the plots. ECC wrote the first draft. All authors read and contributed to the final version of the manuscript.

Disclosures

The authors declare no conflicts of interest.

6. References

References

1. D. H. Auston, "Subpicosecond electrooptic shock-waves," Appl. Phys. Lett. **43**, 713–715 (1983).
2. D. H. Auston and K. P. Cheung, "Coherent time-domain far-infrared spectroscopy," J. Opt. Soc. Am. B-Opt. Phys. **2**, 606–612 (1985).
3. A. Khalid, G. Dunn, R. Macpherson, S. Thoms, D. Macintyre, C. Li, M. Steer, V. Papageorgiou, I. Thayne, M. Kuball *et al.*, "Terahertz oscillations in an In0.53Ga0.47As submicron planar Gunn diode," J. Appl. Phys. **115**, 114502 (2014).
4. A. Biswas, S. Sinha, A. Acharyya, A. Banerjee, S. Pal, H. Satoh, and H. Inokawa, "1.0 thz gan impatt source: Effect of parasitic series resistance," J. Infrared, Millimeter, Terahertz Waves **39**, 954–974 (2018).

5. J. Faist, F. Capasso, D. L. Sivco, C. Sirtori, A. L. Hutchinson, and A. Y. Cho, "Quantum cascade laser," Science **264**, 553–556 (1994).
6. G. Scalari, C. Walther, M. Fischer, R. Terazzi, H. Beere, D. Ritchie, and J. Faist, "THz and sub-THz quantum cascade lasers," Laser Photon. Rev. **3**, 45–66 (2009).
7. F. Lambert, E. Reyes-Reyes, G. Hernandez-Cardoso, A. Gomez-Sepulveda, and E. Castro-Camus, "In situ determination of the state of conservation of paint coatings on the kiosk of guadalajara using terahertz time-domain spectroscopy," J. Infrared, Millimeter, Terahertz Waves pp. 1–10 (2019).
8. C. L. K. Dandolo, M. Lopez, K. Fukunaga, Y. Ueno, R. Pillay, D. Giovannacci, Y. Le Du, X. Bai, M. Menu, and V. Detalle, "Toward a multimodal fusion of layered cultural object images: complementarity of optical coherence tomography and terahertz time-domain imaging in the heritage field," Appl. optics **58**, 1281–1290 (2019).
9. C. L. K. Dandolo, G. M. P. Saldaña, M. A. I. Caballero, M. A. G. Sepúlveda, A. I. Hernández-Serrano, A. M. Orozco, J. A. Calderón, M. S. C. Zárate, K. L. González, E. C. P. de Dios *et al.*, "Terahertz time-domain imaging to guide a conservation intervention on a stratified easel painting," J. Infrared, Millimeter, Terahertz Waves **39**, 773–784 (2018).
10. A. K. Singh, A. V. Pérez-López, J. Simpson, and E. Castro-Camus, "Three-dimensional water mapping of succulent agave victoriae-reginae leaves by terahertz imaging," Sci. Reports **10**, 1–9 (2020).
11. R. Gente and M. Koch, "Monitoring leaf water content with thz and sub-thz waves," Plant methods **11**, 15 (2015).
12. G. Hernandez-Cardoso, S. Rojas-Landeros, M. Alfaro-Gomez, A. Hernandez-Serrano, I. Salas-Gutierrez, E. Lemus-Bedolla, A. Castillo-Guzman, H. Lopez-Lemus, and E. Castro-Camus, "Terahertz imaging for early screening of diabetic foot syndrome: A proof of concept," Sci. Reports **7**, 42124 (2017).
13. Q. Sun, Y. He, K. Liu, S. Fan, E. P. Parrott, and E. Pickwell-MacPherson, "Recent advances in terahertz technology for biomedical applications," Quant. imaging medicine surgery **7**, 345 (2017).
14. M. Browne, N. T. Yardimci, C. Scoffoni, M. Jarrahi, and L. Sack, "Prediction of leaf water potential and relative water content using terahertz radiation spectroscopy," Plant Direct **4**, e00197 (2020).
15. K. Kawase, T. Shibuya, S. Hayashi, and K. Suizu, "THz imaging techniques for nondestructive inspections," Comptes Rendus Physique **11**, 510–518 (2010).
16. S. Katletz, M. Pfleger, H. Pühringer, M. Mikulics, N. Vieweg, O. Peters, B. Scherger, M. Scheller, M. Koch, and K. Wiesauer, "Polarization sensitive terahertz imaging: detection of birefringence and optical axis," Opt. express **20**, 23025–23035 (2012).
17. T. Nagatsuma, G. Ducournau, and C. C. Renaud, "Advances in terahertz communications accelerated by photonics," Nat. Photonics **10**, 371 (2016).
18. R. Piesiewicz, T. Kleine-Ostmann, N. Krumbholz, D. Mittleman, M. Koch, J. Schoebei, and T. Kurner, "Short-range ultra-broadband terahertz communications: Concepts and perspectives," IEEE Antennas Propag. Mag. **49**, 24–39 (2007).
19. T. Kleine-Ostmann and T. Nagatsuma, "A review on terahertz communications research," J. Infrared, Millimeter, Terahertz Waves **32**, 143–171 (2011).
20. H.-J. Song, K. Ajito, Y. Muramoto, A. Wakatsuki, T. Nagatsuma, and N. Kukutsu, "24 gbit/s data transmission in 300 ghz band for future terahertz communications," Electron. Lett. **48**, 953–954 (2012).
21. Y. Monnai, K. Altmann, C. Jansen, H. Hillmer, M. Koch, and H. Shinoda, "Terahertz beam steering and variable focusing using programmable diffraction gratings," Opt. express **21**, 2347–2354 (2013).
22. M. R. M. Hashemi, S.-H. Yang, T. Wang, N. Sepúlveda, and M. Jarrahi, "Electronically-controlled beam-steering through vanadium dioxide metasurfaces," Sci. reports **6**, 35439 (2016).
23. B. Scherger, M. Reuter, M. Scheller, K. Altmann, N. Vieweg, R. Dabrowski, J. A. Deibel, and M. Koch, "Discrete terahertz beam steering with an electrically controlled liquid crystal device," J. Infrared, Millimeter, Terahertz Waves **33**, 1117–1122 (2012).
24. S. Busch, B. Scherger, M. Scheller, and M. Koch, "Optically controlled terahertz beam steering and imaging," Opt. letters **37**, 1391–1393 (2012).
25. T. P. Steinbusch, H. K. Tyagi, M. C. Schaafsma, G. Georgiou, and J. G. Rivas, "Active terahertz beam steering by photo-generated graded index gratings in thin semiconductor films," Opt. express **22**, 26559–26571 (2014).
26. K. Uematsu, K.-i. Maki, and C. Otani, "Terahertz beam steering using interference of femtosecond optical pulses," Opt. express **20**, 22914–22921 (2012).
27. H. Füser and M. Bieler, "Terahertz beam steering by optical coherent control," Appl. Phys. Lett. **102**, 251109 (2013).
28. E. Castro-Camus, M. Koch, and A. I. Hernandez-Serrano, "Perspective: Additive manufacture of photonic components for the terahertz band," J. Appl. Phys. **127**, in press (2020).
29. J. Colla, R. Vickers, M. Nancarrow, and R. Lewis, "3D printing metallised plastics as terahertz reflectors," J. Infrared, Millimeter, Terahertz Waves pp. 1–11 (2019).
30. J. Liu, R. Mendis, and D. M. Mittleman, "A maxwell's fish eye lens for the terahertz region," Appl. Phys. Lett. **103**, 031104 (2013).
31. A. Hernandez-Serrano, M. Weidenbach, S. Busch, M. Koch, and E. Castro-Camus, "Fabrication of gradient-refractive-index lenses for terahertz applications by three-dimensional printing," JOSA B **33**, 928–931 (2016).
32. Z. Wu, J. Kinast, M. Gehm, and H. Xin, "Rapid and inexpensive fabrication of terahertz electromagnetic bandgap structures," Opt. Express **16**, 16442–16451 (2008).
33. A. Sadeqi, H. R. Nejad, and S. Sonkusale, "3D printed metamaterials for high-frequency applications," in *Terahertz, RF, Millimeter, and Submillimeter-Wave Technology and Applications XII,* vol. 10917 (International Society for

Optics and Photonics, 2019), p. 1091708.
34. A. Squires, E. Constable, and R. A. Lewis, "3D printed terahertz diffraction gratings and lenses," J. Infrared, Millimeter, Terahertz Waves **36**, 72–80 (2015).
35. S. F. Busch, M. Weidenbach, J. C. Balzer, and M. Koch, "THz optics 3D printed with topas," J. Infrared, Millimeter, Terahertz Waves **37**, 303–307 (2016).
36. W. D. Furlan, V. Ferrando, J. A. Monsoriu, P. Zagrajek, E. Czerwińska, and M. Szustakowski, "3D printed diffractive terahertz lenses," Opt. letters **41**, 1748–1751 (2016).
37. J. Suszek, A. Siemion, M. S. Bieda, N. Błocki, D. Coquillat, G. Cywiński, E. Czerwińska, M. Doch, A. Kowalczyk, N. Palka *et al.*, "3-d-printed flat optics for THz linear scanners," IEEE transactions on Terahertz Sci. Technol. **5**, 314–316 (2015).
38. Z. Zhang, X. Wei, C. Liu, K. Wang, J. Liu, and Z. Yang, "Rapid fabrication of terahertz lens via three-dimensional printing technology," Chin. Opt. Lett. **13**, 022201–022201 (2015).
39. K. Szkudlarek, M. Sypek, G. Cywiński, J. Suszek, P. Zagrajek, A. Feduniewicz-Żmuda, I. Yahniuk, S. Yatsunenko, A. Nowakowska-Siwińska, D. Coquillat *et al.*, "Terahertz 3D printed diffractive lens matrices for field-effect transistor detector focal plane arrays," Opt. express **24**, 20119–20131 (2016).
40. A. Siemion, "Terahertz diffractive optics?smart control over radiation," J. Infrared, Millimeter, Terahertz Waves **40**, 477–499 (2019).
41. S. Busch, M. Weidenbach, M. Fey, F. Schäfer, T. Probst, and M. Koch, "Optical properties of 3D printable plastics in the THz regime and their application for 3D printed THz optics," J. Infrared, Millimeter, Terahertz Waves **35**, 993–997 (2014).